Probability Density Function of Bubble Size Based Reagent Dosage Predictive Control for Copper Roughing Flotation

Jianyong Zhu[a,b], Weihua Gui[a], Chunhua Yang[a], Honglei Xu[a,c], Xiaoli Wang[a]

a. School of Information Science and Engineering, Central South University, Hunan 410083, China.

b. Nanchang Campus, JiangXi University of Science and technology, Nanchang 330029,China

c. Department of Mathematics and Statistics, Curtin University, Perth WA, 6845, Australia

Abstract:

As an effective measurement indicator of bubble stability, bubble size structure is believed to be closely related to flotation performance in copper roughing flotation. Moreover, reagent dosage has a very important influence on the bubble size structure. In this paper, a novel reagent dosage predictive control method based on probability density function (PDF) of bubble size is proposed to implement the indices of roughing circuit. Firstly, the froth images captured in the copper roughing are segmented by using a two-pass watershed algorithm. In order to characterize bubble size structure with non-Gaussian feature, an entropy based B-spline estimator is hence investigated to depict the PDF of the bubble size. Since the weights of B-spline are interrelated and related to the reagent dosage, a multi-output least square support vector machine (MLS-SVM) is applied to establish a dynamical relationship between the weights and the reagent dosage. Finally, an entropy based optimization algorithm is proposed to determine reagent dosage in order to implement tracking control for the PDF of the output bubble size. Experimental results can show the effectiveness of the proposed method.

Keyword: froth flotation, B-spline, reagent dosage, predictive control, bubble size, probability density function, MLS-SVM

1 Introduction

Froth flotation is the most important method to separate valuable minerals from ore by means of the physical and chemical properties of mineral surfaces. Generally, flotation reagents to improve or decrease mineral's flotability are added to make effective separation of valuable minerals. In fact, the reagent dosage has a critical influence on successful flotation. On one hand, less reagent dosage decreases valuable mineral's flotability, and results in lower concentrate grade and recovery of the plant. Excessive reagent dosage, on the other hand, is likely to lead to worse grade (or recovery) and cause the product deficit. In addition, an increase of 1%~2% in recovery or grade is economically remarkable in copper flotation plants. Therefore, the reagent dosage control is a very important aspect of the flotation strategy in commercial plants.

In recent years, the reagent dosage control has attracted great interest of both academic and industrial researchers. In Hodouin et al. (2000) a feedforward and feedback prediction control algorithm was developed to control the reagent dosage. The reagent addition is determined according to ore amount and property by using a feedforward control strategy, and then the dosage is moderately adjusted by feedback control. It also shows that optimization and control of mineral

---

Corresponding author. Tel.: +8613908462048. Fax: :86-0731-88710482

E-mail address: jianyong-zhu@csu.edu.cn(Jianyong Zhu), gwh@csu.edu.cn(Weihua Gui)

processing couldn't be performed without a minimum amount of information on the input disturbances, the process states, and the final product quality. In Naik et al. (2005) a regression model is established to predict the grade and recovery of combustible material for different reagent conditions by quantifying the effect of sodium meta silicate, collector and frother with factorial experiment data. In Suichies et al. (2000) a generalized predictive control (GPC) algorithm is presented and this algorithm has been applied to many sulfide flotation circuits in the Brunswick mining concentrator. It has proved that the GPC controller performs well on the flotation circuits. Although MPC seems to be the ideal solution for high quality control, Bergh and Yianatos (2011) indicates that the benefits of MPC should not be lost without the actual plant constraints.

In practice, the operators of flotation plant monitor and optimize reagent additions of the flotation process mainly by observing the froth appearance characteristics such as bubble size and color owing to the lack of testing equipments such as X-ray fluorescence analyzers. Conventionally, the reagent dosage control heavily depends on the frequent inspection of froth views and manipulation of experienced operators, which often causes serious delayed responses. In Kaartinen et al. (2006), the correlations between recovery and froth appearance characteristics is established and subsequently a rule-based feedback control strategy is designed. It is shown that the image-based reagent dosage control strategy is possible to achieve considerable financial benefits in terms of improved recovery.

As one of the dominant visual features, bubble size structure has a great effect on the probability of collision between mineral particles and bubbles, as well as the adhesion of the particles to the bubbles (Aldrich and Feng, 2000). Flotation kinetics shows that the transfer processes of mineral particles take place in the pulp phase (from the pulp phase to the froth phase) and in the froth phase (from the froth phase to the concentrate launder) by particle–bubble attachment. All of these sub processes depend strongly on bubble size. If the bubble size is too large, the bubbles easily burst, and the valuable mineral particles attached the burst bubbles will fall into the tailings, resulting in the reduction of recovery. And vice versa. As an effective indicator of bubble stability, bubble size structure is believed to be closely related to flotation performance since the bubble size reflects the extent of bubble coalescence. Many researchers have investigated the relationship between the bubble size and water recovery, froth recovery, etc. For example, Neethling et al. (2003) shows that bubble size determines water recovery with an inverse squared relationship.

It is noticed that the observable bubble size is really the film bubble size on the top of the froth. The bubble size in the collection zone named 3D bubble size is hardly measured in industrial flotation machine, but is capable to be observed and measured in laboratory flotation machine. Wang and Neethling (Wang and Neethling, 2009) explores the relationship between the film bubble size and the 3D bubble size and proved that the difference between film bubble size distribution and 3D bubble size distribution are not remarkable such that the mentioned bubble size distribution in the paper is really the film bubble size distribution.

It is beyond doubt that bubble size is a key parameter in froth flotation. Bubble size closely relates to the operation parameters such as airflow rate, impeller speed, pulp level, reagent dosage (Grau and Heiskanen, 2005). Little changes of the impeller speed and the airflow rate will have

less effect on bubble size for Wemco's flotation cell with self-aspirating aeration mechanisms (Girgin et al., 2006). Among them, the reagent dosage has very important influence on bubble size. It is commonly believed that the bubble size decreases with an increase in the froth concentration owing to a decrease in the surface tension induced by the addition of surfactants, and at a particular concentration, the bubble size levels off. In Cho and Laskowski (2002) the researchers suggest that the frothers control bubble size by reducing bubble coalescence in the cell and that coalescence be entirely prevented at concentrations exceeding the critical coalescence concentration (CCC) in a dynamic system. In addition to the frother, the collectors also have an influence upon coalescence and evaporation of bubbles by interacting with the frother.

Bubble size presents characteristics of random distribution in flotation process. And it is worth noticing that the PDF of bubble size has been found to be non-Gaussian distribution (Yang, Xu, et al., 2009). Generally, researchers tend to focus on singular statistical features of bubble size such as mean, standard deviation, kurtosis and skewness to characterize bubble size structure. However, it is well known that the features are incapable to represent the entire profile of bubble size distribution with non-Gaussian feature.

Except the well-developed minimum variance control, LQG and mean value control, some researchers explore other random variable distribution control algorithms in order to implement control and diagnosis of variables with non-Gaussian distribution. In Wang (2000) adopted B-spline expansions are developed to model PDF of variables with non-Gaussian and subsequently a BSD based control algorithm is constructed to track the given PDF. In Guo and Wang (2010) some further innovative and systematical work on modeling and system analysis is conducted including the structure controller design and fault detection and diagnosis for non-Gaussian distribution. In Forbes et al. (2004) Gram-Charlier based PDF parameterization method is proposed and regulatory control synthesis techniques for shaping the PDF of stochastic process is developed. Weight dynamic model built in Wang (2000), Guo and Wang (2010), Forbes et al. (2004) is limited to precise linear systems, so these methods are not suitable for the flotation process with highly nonlinear and complex mechanism. In Yang, Guo, and Wang (2009), a constrained proportional-integral (PI) tracking control for probability distribution of the output variable is proposed based on two step neural networks. Although dynamic relationship between the control input and the weights is built by using dynamic neural network in Yang, Guo, and Wang (2009), the method which is applied to a linear system is difficult to be directly used for the flotation process. In Xu, Gui et al. (2011) a flotation process fault detection system based on output PDF of bubble size distribution is designed, where the distribution is described by a kernel estimation method. Recently, in Liu, Gui et al. (2013) dynamic bubble size distribution is used to recognize operate state of reagent addition in copper flotation process.

This work aims to develop bubble size PDF based reagent dosage control for roughing flotation of Copper flotation plants. Based on PDF modeling work using B-Spline estimator (Wang, 2000; Guo and Wang, 2010; Yang, Guo, and Wang, 2009; Forbes et al., 2004), an entropy based B-Spline estimation technique is investigated to depict the PDF model according to bubble size extracted from froth images of copper flotation. Based on the analysis of the flotation process, PDF of bubble size based reagent dosage predictive control method is firstly proposed to implement the indices of the roughing flotation. The method abundantly takes advantage of the

fact that bubble size structure closely relates to the indices and responds to changes in the reagent dosage. The novelty of this proposed approach is that the method is using PDF of bubble size rather than a concentrate grade or recovery as a target variable. In addition, instead of by using flotation mechanism, the proposed reagent dosage control method is built by integrating machine vision, random distribution control and predictive control principle. As such, a MLS-SVM model is firstly proposed to establish the relationship between the reagent dosage and bubble size. In order to implement the tracking of the targeted PDF, an entropy based optimization algorithm is then proposed to calculate the reagent dosage.

The rest of the paper is organized as follows: a copper flotation circuit of a copper flotation plant is described in Section 2; Section 3 proposes the bubble size PDF based reagent dosage predictive control to implement PDF tracking of the output bubble size. Experimental results and discussions are presented in Section 4. Section 5 illustrates the conclusion and directions for future research.

2 Process description and modeling analysis

2.1 Process description of copper flotation

A concise flow diagram of the copper flotation process can be shown in Fig.1. Raw ore is firstly conveyed to the ball milling. Next, the ball milling breaks the feeding ore into pulp slurry with a suitable particle size (minerals size should be under 200 mesh, i.e., less than 0.074mm). Eligible slurry from ball milling is then fed into an agitated tank, where the valuable mineral particles are selectively coated with hydrophobic chemicals. After being fully agitated, the slurry is fed into flotation cells with self-aspirating aeration mechanisms, where air together with frothing reagents produces a large number of stable bubbles, which travel to the surface of the froth due to buoyancy, carry the valuable mineral particles for their hydrophobicity, and form a froth layer. The valuable mineral particles are skimmed from the froth layer by using natural overflow typically called the concentrate flow. The remaining slurry in the flotation cell will be discharged from the bottom of the flotation cell, resulting in the tailing flow.

The copper flotation process contains the roughing circuit, the scavenging circuit and the cleaning circuit. These circuits will ensure both high grade in the final product and high overall recovery. In order to improve recovery efficiency, the concentrate of the scavenging and the tailing of the cleaning need to be regrinded for re-flotation. Each circuit is used to separate the specific mineral particles from other particles and has an individual 'role'. For example, the roughing circuit carries out more easily floated valuable mineral particles from the gangue by adding Z200. The scavenging circuit separates hard-flotation valuable mineral particles from the gangue by adding butyl xanthates and BC. Therefore, the recovery is more important than the grade in the two circuits. The cleaning circuit, on the other hand, produces the final product, and therefore the grade of the concentrate becomes more important than the recovery.
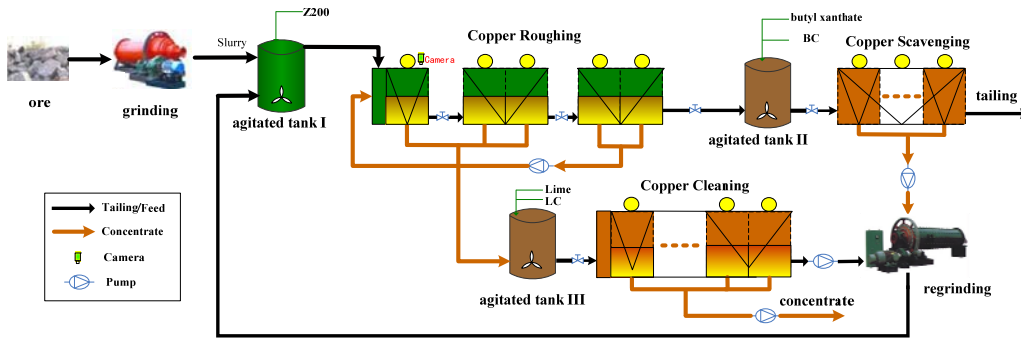
Fig.1. Flow diagram of copper flotation process

2.2 Modeling analysis of reagent dosage control

As the experienced operators point out, the reagent dosage control of the roughing circuit directly affecting product indices of subsequent flotation circuit such as scavenging circuit and clearing circuit plays a vital role for the overall control strategy. If the reagent dosage is unsuccessfully tuned in roughing circuit, the product indices of subsequent circuits are hardly implemented no matter how their operation parameters are adjusted. Therefore, the first cell of copper roughing circuit in which most reagent dosages are added is usually taken as a control object.

In addition, it is noticing that the feed parameters (such as feed grade, feed flow rate, solid percent, particle size of solid and pH, etc.) modify the flotation performance. Firstly, the criterion of bubble size is closely related to the ore grade. If the ore grade fluctuates markedly, the corresponding reagent dosage need to be regulated and the criterion of the optimal PDF of the bubble size also varies under the same handling capacity of the raw ore. So the ore property is a prerequisite for reagent dosage control. Secondly, feed flow rate, pulp concentration and particle size of solid from grinding should be necessary condition for successful flotation. The parameters vary at all times. If the parameters are properly controlled in the grinding circuit, they will keeps relatively stable and good running of the flotation also keeps relatively stable. Otherwise, the operation variables of flotation need to be regulated to meet production indices of flotation. So the parameters are considered to be disturbance variables.

Although developments in the mineral process industry have been made in hardware as well as in software, It has proved that the development of flotation mechanism model based robust reagent dosage control system for flotation circuits is quite difficult. Reasons for this include the inherent complexity, dynamics and nonlinearity of flotation, the lack of testing equipments such as X-ray fluorescence analyzers and unpredictability of the response of most flotation circuits to upset conditions. Hodouin et al. (2001) emphasized that mineral processing optimization and control could not be performed without a minimum amount of information on the input disturbances, the process states, and the final product quality.

Bubble size structure reflects important process characteristics and responds to changes in the reagent dosage. Therefore, by employing bubble size as process outputs, it is possible to build a causal process model that can predict bubble size from the given values of the reagent dosage and the historical data of bubble size. With this model, the new values of the reagent dosage for achieving specified bubble size distribution can be obtained via optimization. The novelty of this

5

approach consisted that instead of using a concentrate grade or recovery as a target variable, the method used PDF of bubble size. Since this model was obtained from reagent dosage and bubble size, no grade measurements are needed.

3 PDF based reagent dosage predictive control

As mentioned above, bubble size of the first cell of roughing circuit is taken as a controlled object and the reagent dosage is taken as a manipulated variable. The ore property may be a prerequisite for reagent dosage control. The other feed parameters such as feed flow rate, pulp concentration and particle size of solid, etc. are taken as disturbances. In addition, the given PDF of bubble size is determined by process tests and expert knowledge in the same condition as ore property. In practice, the experienced and expert workers monitor flotation running by observing bubble size structure. When bubble size is capable to reflect very good grade according to the workers' experience and expert knowledge during good flotation running, the froth image is captured and processed to be a PDF of bubble size, and the corresponding froth is simultaneously collected and then assayed. As such, a group of data including PDF of bubble size and the corresponding froth grade are obtained. Through a lot of process tests, a great number of groups are obtained. The probability density functions (PDFs) of bubble size are selected and then analyzed to determine the desire PDF of the bubble size by the regression technology if the corresponding froth grade is relatively high.

3.1 Model structure

The proposed reagent dosage predictive control model structure shown in Fig. 2 mainly consists of a measurement unit, a multi-output least square support vector machine (MLS-SVM) unit, a feedback correction unit and a reagent dosage optimization control unit. The froth image captured by an industrial camera is segmented into bubble size set by the proposed segment algorithm in the measurement unit. And then the output PDF of bubble size can be estimated by a minimum entropy based B-spline method and be formulated by

$$r(y,w) = \sum_{i=1}^{n} w_i B_i(y) = [B_1(y), B_2(y), \cdots, B_n(y)][w_1, w_2, \cdots, w_n]^T = C(y)V \tag{1}$$

where $r(y,w)$ represents the PDF of bubble size. $B_i(y)$ is the base function with give order of the B-spline. w_i represents the corresponding weights. n is the number of B-spline functions. $C(y) = [B_1(y), B_2(y), \cdots, B_n(y)]$ and $V = [w_1, w_2, \cdots, w_n]^T$. Since the B-spline consists of the base functions and the corresponding weights, the PDF can be characterized by the weight vector of B-spline if the base functions of B-spline are all fixed. So, the output weight vector of the measurement unit at time k can be represented as $V_o(k) = [w_{o1}(k), w_{o2}(k), \cdots, w_{on}(k)]^T$.
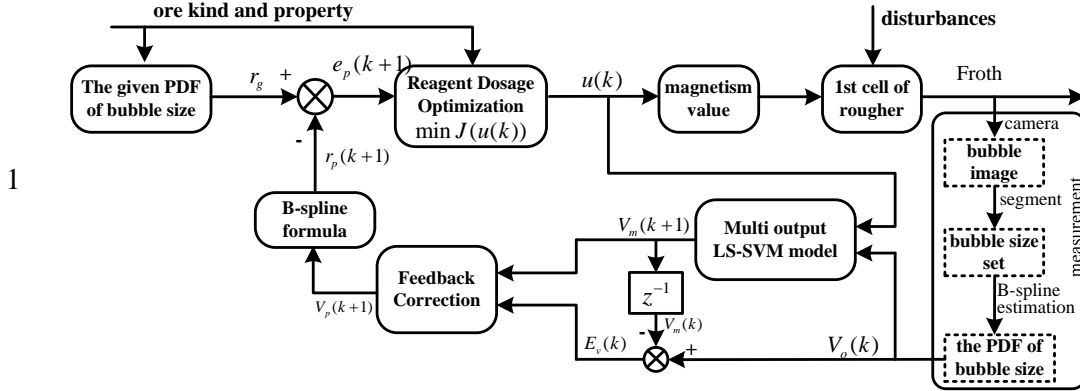
Fig.2. Proposed reagent dosage predictive control structure

In Fig.2, the inputs of MLS-SVM model are the reagent dosage $u(k)$ and the output weight vector $V_o(k)$. The predictive weight vector of MLS-SVM model at time k can be formulated as

$$V_m(k+1) = f(u(k), V_o(k)) \qquad (2)$$

where $V_m(k+1) = [w_{m1}(k+1), w_{m2}(k+1), \cdots, w_{mn}(k+1)]^T$, $f(\cdot)$ represents a nonlinear function. According to Eq.(1) and Eq.(2), the predictive PDF of MLS-SVM model at time k can be formulated as

$$r_m(k+1) = C(y)V_m(k+1) = C(y) \bullet f(u(k), V_o(k)) \qquad (3)$$

It is obvious that $r_m(k+1)$ only relates to the reagent dosage $u(k)$ and the output weight vector $V_o(k)$ at time k if the vector $C(y)$ is fixed.

In order to inhibit the accumulated error of the output weight vector and improve predictive accuracy, the feedback correction unit is designed. The output of the unit is formulated as

$$V_p(k+1) = V_m(k+1) + E_v(k) = V_m(k+1) + V_m(k) - V_o(k)$$

(4)

where $V_p(k+1) = [w_{p1}(k+1), w_{p2}(k+1), \cdots, w_{pn}(k+1)]^T$, $E_v(k)$ represents the error between the predictive weight vector of the MLS-SVM and the weight vector of the output PDF of bubble size at time k.

By using B-spline formula, $r_p(k+1)$ can be written as

$$r_p(k+1) = C(y)V_p(k+1) \qquad (5)$$

It is obvious that $r_p(k+1)$ only relates to history reagent dosages and output weight vectors if the vector $C(y)$ is fixed. $e_p(k+1)$ will be

$$e_p(k+1) = r_g - r_p(k+1) \qquad (6)$$

where r_g is the given PDF.

3.2 PDF of bubble size based on B-spline

3.2.1 Froth image segment

The froth image captured by the camera needs to be segmented. Recently, a great number of methods have been reported to segment the froth images including valley-edge detection and tracing techniques (Wang, Bergholm and Yang 2003), white spots detection (Wang and Li 2005),

7

watershed transformation (Bartolacci et al. 2001) and wavelet approach (Liu, Macgregor et al. 2005). However, these methods cannot effectively deal with the copper froth image with large and tiny bubbles. In Runge et al. (2007), it is pointed out that the watershed algorithm in VisioFroth is unable to successfully delineate the bubbles when both large and tiny bubbles were present in a froth image. Botha (1999) shows that the marker of bubble area ratio can be used to determine areas of tiny bubbles. And the texture measure of small number emphasis could be used to determine areas of tiny bubbles. However, this method was deemed unfeasible for our froth image segment due to excessive computation time and the sensitivity to various parameters.

In Forbes (2007), a two-pass watershed algorithm is explored to localize areas of the froth image with both large and tiny bubbles such that the areas with large and tiny bubbles are processed with different parameters of watershed algorithm. The bubbles in Fig. 3(c) which are all more or less of the same size are easy to be segmented. And the bubbles in Fig. 3(a) and 3(b) containing both big and tiny bubbles are accurately segmented by the proposed method. Overall, Fig. 3 can show that the algorithm can achieve good segmentation under such conditions.

| (a) | (b) | (c) |
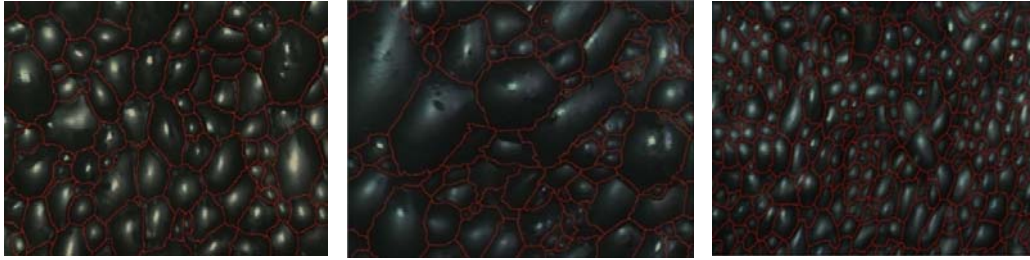
Fig.3 Froth image is segmented by the proposed method.(a) big and small bubbles (b) large and tiny bubbles (c) medium and small bubbles

3.2.2 Entropy based B-spline estimation for bubble size

The distribution of some random variables can be well approximated by Gaussian, Exponential, Weibull distribution and etc. However, the distribution of many other random variables such as flotation BSD and paper flocculation size distribution cannot be approximated by those simple distribution forms. Instead of using basic distributions, some authors have developed nonparametric estimation techniques such as histogram, frequency polygon, shift average histogram, kernel method, wavelet method and B-spline model.

Among them, the B-spline based estimation method can be used to identify an appropriate PDF of a random variable from a given sample of data. For a dynamic stochastic system, $\eta(t) \in [a,b]$ as the stochastic output and the probability of output $r(y)$ lying inside $[a,\sigma]$ can be described as

$$P(a \le \eta(t) \le \sigma) = \int_a^\sigma r(y)dy \tag{7}$$

where $r(y)$ is output PDF of the stochastic variable $\eta(t)$.

The PDF $r(y,w)$ of a continuous random variable Y can be formulated as

$$r(y,w) = \sum_{i=1}^n w_i B_i(y) \tag{8}$$

where w_i represent the weights, n is the number of B-spline functions used to approximate the

8

PDF. $B_i(y)$ is the base function with give order of the B-spline. The second order B-spline function is in the form of

$$B_j(y) = (y_j - y_s) \sum_{t=0}^{3} \frac{(y_{s+t} - y)^2 H(y_{s+t} - y)}{w_s'(y_{s+t})} H(y - y_s) \tag{9}$$

$$w_s(y) = \prod_{u=0}^{3} (y - y_{s+u}) \tag{10}$$

where $H(y)$ is Heaviside function and $s = j - 3$ (Zong and Lam, 1998) . The distribution range of Y is $[c,d]$. Divide the range $[c,d]$ into n equal divisions. The division points are called the nodes of B-spline functions and denoted by y_i, which satisfy

$c = y_0 < y_1 < y_2 < \cdots < y_n < d$

For convenience of calculation, assume that there are two extended nodes y_{-2}, y_{-1} and y_{n+1}, y_{n+2} exist at each end, Let $y_{-1} = y_{-2} = y_0$ and $y_{n+1} = y_{n+2} = y_n$. The PDF in (8) should satisfy two conditions. The first condition is that the weight w_i should be greater than zero so that the PDF is always positive in the distribution range. The second condition is that the integral of $r(y,w)$ over $(-\infty, +\infty)$ should be one, i.e.,

$$\int_{-\infty}^{+\infty} r(y,w)dx = \sum_{j=1}^{N} w_j \int_{y_{j-3}}^{y_j} B_j(y)dx = \sum_{j=1}^{N} w_j \frac{y_j - y_{j-3}}{3} = 1 \tag{11}$$

Thus, in order to find the best model from a set of candidate statistical models, the asymptotically unbiased estimate of PDF will be

$$ME = \frac{3n_f}{2n_s} - \int r(y|a) \cdot \log r(y|a)\, dy \tag{12}$$

where n_s is the number of sample points, n_f is the number of free parameters in the model and equals to N-1 in light of the equality constraint in Eq. (11), and a is the maximum likelihood estimate of a.

According to (12) by minimizing measured entropy, the weights will be obtained in the form of

$$w_j = \frac{1}{n_s c_j} \times \sum_{l=1}^{n_s} \frac{w_j B_j(y_l)}{r(y,u)} \tag{13}$$

where $c_j = (y_j - y_{j-3})/3$, n_s presents the amount of given sample, and $B_j(y_l)$ denotes the base function.

Bubble size of every segmented region represents the amount of pixels in the region in term of a froth image. Before estimation, bubble size is normalized in order to implement PDF estimation of bubble size. The PDF of bubble size approximated by B-spline function and kernel is shown in Fig. 4(a). Blue lines represent the base functions of B-spline. Blue dotted lines represent intermediate functions, which are determined by means of multiplying base functions by corresponding weight values. Red line represents the PDF of bubble size obtained by summation of intermediate functions. Green line represents the kernel estimation based PDF of bubble size. It is shown that all the typical froth size distributions in rough cells tend to have a long tail with skewness to the left.

As for post segmentation analysis, the number of base functions is essential to depict accurately PDF of bubble size. The influence of the B-spline number is shown in Fig. 4(b). When

1   the numbers of base functions are five and seven, the accuracy will be low and the estimated PDF

2   can only roughly exhibit the distribution. When the numbers are fifteen and twenty, the estimated

3   PDF has several peaks, which should be excluded. When the numbers are nine, the estimated PDF

4   has the best accuracy. A large number of flotation froth images are applied to PDF estimation of

5   bubble size, and then the results show that the optimal number of base functions is nine. It is seen

6   from the measured entropy analysis proposed in the above sections that the estimation has the best

7   accuracy and is very close to the given one when the number is nine.

8
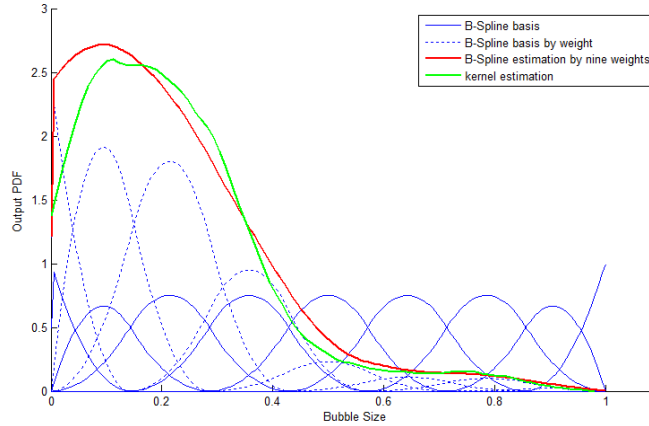
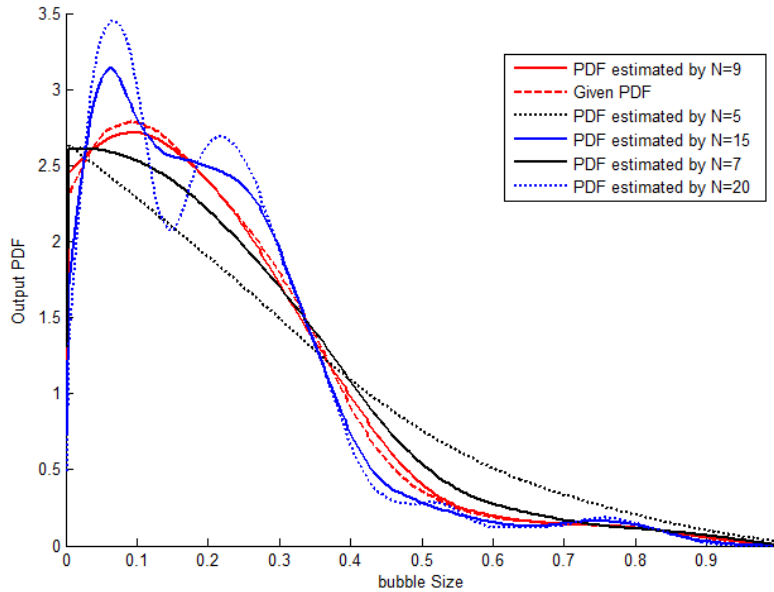9   (a)

10

11   (b)

12   Fig.4 PDF estimation by entropy based B-spline technology. (a) PDF estimation by B-Spline and kernel (b) PDF

13   estimation by entropy based B-spline technology, where N presents the B-spline number

3.3   Multi-output LS-SVM based nonlinear model

15   The nonlinear prediction unit in Fig.2 is capable to use principle component analysis (PCA),

16   partial least squares (PLS), independent component analysis (ICA), fisher discriminant analysis

17   (FDA), subspace aided approach (SAP) , LS-SVM and neural networks, etc. One basic

18   assumption for successful application of PCA, PLS and FDA related approaches in the steady

state is that the process data follow multivariate Gaussian distribution and SAP has relatively high computation cost (Yin, Ding, et al., 2012). Compared with the methods, LS-SVM has a simple topological structure and good generalization capacity and replaces convex quadratic programming problem with convex linear system solving problem, thus largely speeding up training.

LS-SVM has been successfully applied to the identification and control of dynamic systems. Despite its potential usefulness, the standard formulation of the LS-SVM could not cope with the multi-output case. The traditional approach in the multi-output case is that the different outputs are formulated by LS-SVM formula. The method disregards the underlying (potentially nonlinear) cross relatedness among different outputs. To overcome the disadvantage, some multi-output LS-SVM methods have been proposed in Xu, An, et al., 2013; Han, Liu, et al., 2012. When different outputs have their relationship, these methods can be advantageous to learn all outputs simultaneously.

3.3.1 Multi-output LS-SVM model

When the weights of the PDF always interact on each other, we can add a combined fitting error to the regression model to measure the effect between these multiple outputs. Giving a training sample set denoted as $S = \{X(k), Y(k+1)\}$, where the input vector $X(k) = [x_1(k), x_2(k), \cdots, x_p(k)]$, $x_i \in R^p$ represents the reagent dosage and nine weights of the output PDF of bubble size at time k, and P is set as 10. The output vector $Y(k+1) = [y^1(k+1), y^2(k+1), \cdots, y^{n_y}(k+1)]$, $y^j \in R^{n_y}$ represents the predictive weight at time k with dimensionality $n_y = 9$. The multi-output LS-SVM (Han, Liu, etc., 2012) can be formulated as follows：

$$Y(k+1) = \mathbf{W}^T \Phi(x(k)) + \mathbf{B} \tag{14}$$

Where $\Phi(x_i) = [\varphi(x_i), \varphi(x_i), \cdots \varphi(x_i)]^T$, where the nonlinear mapping $\varphi(x_i)$ converts the input data into a high-dimension space. $\mathbf{W}_i$ is a diagonal matrix denoted as $diag(w_i^1, w_i^2, \cdots, w_i^{n_y})$, where w_i^j represents the weight. $\mathbf{B}$ is bias vector denoted as $\mathbf{B} = [b^1, b^2, \cdots, b^{n_y}]^T$, where b^j represents the bias. Compared to the single-output model, all of the variables in this model are in the form of matrix.

Enlightened by the computation of single-output LS-SVM, we can consider an optimization problem with constrains of the multi-output one, where the errors come from not only each single output, but also the combined fitting error. The optimization problem can be described as

$$\min J\left(w^j, b^j, e^j, E_i\right) = \frac{1}{2} \sum_{j=1}^{n_y} \left(w^j\right)^T \left(w^j\right) + \frac{1}{2} \sum_{j=1}^{n_y} \sum_{i=1}^{n} \gamma^j \left(e^j\right)^2 + \gamma^0 \sum_{i=1}^{n} \mathbf{E}_i \tag{15}$$

$$\text{s.t.} \quad y^j = \left(w^j\right)^T \varphi(x) + b^j + e^j \quad j = 1, 2, \ldots, n_y \tag{16}$$

$$\mathbf{E}_i = \left\| \mathbf{Y}_i - \mathbf{W}^T \Phi(x_i) - \mathbf{B} \right\|^2 \quad i = 1, 2, \ldots, n \tag{17}$$

1 where w_i^j and b^j are the weight and bias, respectively. e^j and $\gamma^j (j=1,\cdots,n_y)$ is the single

2 fitting error and the corresponding penalty coefficient, respectively. $\mathbf{E}_i$ and γ^0 represents the

3 combined fitting errors and the penalty coefficient. n represents total number of samples. $\mathbf{Y}_i$ is

4 the output vector.

5 To solve the optimization problem, the following Lagrangian function can be constructed,

6
$$L\left(w^j,b^j,e^j,E_i,\lambda_i,\mu_i^j\right)=\frac{1}{2}\sum_{j=1}^{n_y}\left(w^j\right)^T\left(w^j\right)+\gamma^0\sum_{i=1}^{n}\mathbf{E}_i$$
$$+\frac{1}{2}\sum_{j=1}^{n_y}\sum_{i=1}^{n}\gamma^j\left(e_i^j\right)^2-\sum_{i=1}^{n}\lambda_i\left(\mathbf{E}_i-\mathbf{Y}_i-\mathbf{W}_i\mathbf{\Phi}(x_i)-\mathbf{B}^2\right)$$

7
$$-\sum_{j=1}^{n_y}\sum_{i=1}^{n}\mu_i^j\left(\left(w_i^j\right)^T\varphi(x_i)+b^j+e_i^j-y_i^j\right) \tag{18}$$

8 where μ_i^j represents the Lagrangian multiplier.

9 According to the Karush-Kuhn-Tucker condition, the partial derivatives of the variables are

10 calculated as follows:

11
$$\begin{cases} \dfrac{\partial L}{\partial w^j}=0\rightarrow w^j-2\mathbf{\varphi}^T\mathbf{D}_\lambda\left[y^j-w^j\varphi-\bar{\mathbf{1}}^T b^j\right]-\mathbf{\varphi}^T\mathbf{\mu}^j=0 \\[2mm] \dfrac{\partial L}{\partial b^j}=0\rightarrow -2\Lambda^T\left[y^j-w^j\varphi-\bar{\mathbf{1}}^T b^j\right]-\bar{\mathbf{1}}\mathbf{\mu}^j=0 \\[2mm] \dfrac{\partial L}{\partial E_i}=0\rightarrow \gamma^0-\lambda_i=0 \\[2mm] \dfrac{\partial L}{\partial e^j}=0\rightarrow \gamma^j\bar{\mathbf{1}}e^j-\bar{\mathbf{1}}\mathbf{\mu}^j=0 \\[2mm] \dfrac{\partial L}{\partial\lambda_i}=0\rightarrow \left\|\mathbf{Y}_i-\mathbf{W}^T\mathbf{\Phi}(x(k))-\mathbf{B}\right\|^2=\mathbf{E}_i \\[2mm] \dfrac{\partial L}{\partial\mu^j}=0\rightarrow \bar{\mathbf{1}}\mathbf{y}^j=\mathbf{w}^j\mathbf{\varphi}+n_y b^j+\bar{\mathbf{1}}e^j \end{cases} \tag{19}$$

12 where the row vector $\bar{\mathbf{1}}=[1\ 1\cdots 1]_{1\times n}$, the column vector $\Lambda=[\lambda_1,\lambda_2,\cdots,\lambda_n]^T$ and the diagonal

13 matrix $D_\lambda=diag(\lambda_1,\lambda_2,\cdots,\lambda_n)$. Considering the undetermined expression of the nonlinear

14 mapping, w^j is transformed into a mapping combination on high- dimension space, i.e.

15
$$w^j=\sum_{i=1}^{n}\alpha_i^j\varphi(x_i')=\mathbf{\varphi}^T\mathbf{\alpha}^j \tag{20}$$

16 and the kernel function with dimensionality $n\times n$, selected as a Gaussian radial basis function, is

17 given by

18
$$\mathbf{K}^j(x_i,x_k)=\mathbf{\varphi}(x_i)\mathbf{\varphi}(x_k)^T=\exp(-\frac{\|x_i-x_k\|}{2\sigma^2}) \tag{21}$$

19 Thus, combining (19)–(21), a full-ranked equation set is obtained to solve α, b and μ

$$\begin{bmatrix} \mathbf{I}+2\mathbf{D}_\lambda & 2\mathbf{D}_\lambda\bar{\mathbf{1}} & \mathbf{I} \\ -2\lambda^{\mathrm{T}}\mathbf{K} & -2\bar{\mathbf{1}}\lambda & \bar{\mathbf{1}}\left(\gamma^j\right)^{-1}\bar{\mathbf{1}} \\ \mathbf{K} & n_y\bar{\mathbf{1}}^{\mathrm{T}} \end{bmatrix}\begin{bmatrix} \boldsymbol{\alpha}^j \\ \mathbf{b}^j \\ \boldsymbol{\mu}^j \end{bmatrix} = \begin{bmatrix} 2\mathbf{D}_\lambda\mathbf{y}^j \\ -2\lambda^{\mathrm{T}}\mathbf{y}^j \\ \mathbf{y}^j \end{bmatrix} \tag{22}$$

Since (22) can be in the form of $AX = B$ and A is an invertible matrix, one can solve (22) as $X = A^{-1}B$. The regression function prediction based on the multi-output LS-SVM can be formulated as

$$f^j(x) = y^j = \sum_{i=1}^n \alpha_i^j \mathbf{K}\left(x, x_i\right) + b^j \qquad j = 1, 2, \ldots, n_y \tag{23}$$

where j is the number of outputs.

Since the weights of the output PDF of bubble size at time k are known when the model is used for prediction, the reagent dosage $u(k)$ is the only unknown variable. Eq. (23) can be written as:

$$y^j = f^j(X(k)) = f^j(u(k)) \qquad j = 1, 2, \cdots, n_y \tag{24}$$

Eq.(24) shows that the output weight of multi output LS-SVM is only related to the reagent dosage $u(k)$.

3.3.2 Parameter optimization

As for the MLS-SVM model, parameters $\boldsymbol{\alpha}^j, \mathbf{b}^j, \boldsymbol{\mu}^j$ can be solved by Eq. (22). Other

parameters of the proposed model include the widths $\sigma^j(j = 1, 2, \cdots, n_y)$ of the Gaussian kernel

and the penalty coefficients $\gamma^j(j = 0, 1, \cdots, n_y)$ of the errors. Parameters optimization methods

such as cross validation with grid-search, Bayesian network optimization, gradient descent algorithm, and particle swarm optimization (PSO) can be applied to obtain these parameters. Among them, the PSO has been successfully applied to function optimization, artificial network training and fuzzy system control, etc. Since the PSO algorithm is robust and fast in solving non-linear, non-differentiable and multi-modal problems, the PSO algorithm is proposed to select the hyper-parameters of the model.

Let $\vec{x}_i = (x_{i,1}, \cdots, x_{i,d}, \cdots, x_{i,D})$ be the ith particle in a D-dimensional space. The best previous position of the ith particle is recorded and represented as $\vec{p}_i = (p_{i,1}, \cdots, p_{i,d}, \cdots, p_{i,D})$, which gives the best fitness value and is also called $pbest$. The index of the best $pbest$ among all the particles is represented by the symbol g. The location P_g is called $gbest$. The velocity for the ith particle is represented as $\vec{v}_i = (v_{i,1}, \cdots, v_{i,d}, \cdots, v_{i,D})$. The PSO algorithm can change the velocity and location of each particle towards its $pbest$ and $gbest$ locations according to Eq. (25) and (26) at each time step (Guo, Yang, et al. 2008),

$$v_{i,d}(t+1) = wv_{i,d}(t) + c_1r_1(P_{i,d} - x_{i,d}(t)) + c_2r_2(P_{g,d} - x_{i,d}(t)) \tag{25}$$

$$x_{i,d}(t+1) = x_{i,d}(t) + v_{i,d}(t+1) \tag{26}$$

where w is the inertia coefficient which is a constant in the interval [0, 1] and can be adjusted in the direction of linear decrease; c_1 and c_2 are the non-negative learning rate; r_1 and r_2 are generated randomly in the interval [0, 1]; $v_{id} \in [-v_{max}, v_{max}]$ and v_{max} is a designated maximum

velocity. The termination criterion for iterations is determined according to whether the maximum generation or a designated value of the fitness has been reached.

Two key factors for determining the optimized parameters should be considered. First, to implement a more stable optimization, the optimized hyper-parameters for MLS-SVM is encoded as $x = (\sigma^1, \sigma^2, \cdots, \sigma^{n_y}, \log \gamma^0, \log \gamma^1, \cdots, \log \gamma^{n_y})$. Second, the fitness of a particle is evaluated by the following formulation: $f_i = Ave_{test-5}$, where f_i is the fitness of particle i, Ave_{test-5} is the average correct rate when the five-fold cross validations with data in the training set for each particle is performed.

3.4 Entropy based reagent dosage optimization model

Suppose there is a dynamic stochastic system with input $u(t) \in R^m$ and output $y(t) \in [a,b]$, the probability of output $y(t)$ lying in $[a,\xi)$ is defined as

$$P(a \le y(t) \le \xi, u(t)) = \int_a^\xi r(y, u(t)) dy \tag{27}$$

where $u(t)$ represents control input such as the reagent dosage, $r(y, u(t))$ represents the output PDF of the stochastic variable $y(t)$ and is also related to $u(t)$. The $r(y, u(t))$ can be approximated by B-spline function,

$$r(y, u \mid \beta) = \sum_{i=1}^n w_i(u) B_i(y) + e_0(y, u(t)) \tag{28}$$

where $B_i(y)$ and $w_i(u)$ are the base functions and the corresponding weights of B-spline, respectively. β presents conditions of PDF (i.e. ore grade). $e_0(y, u(t))$ is the approximation error satisfying $\|e_0(y, u(t))\| \le \delta_0$, where δ_0 is a known small constant. It is noted that weight $w_i(u)$ is related to the reagent dosage $u(t)$. Since $r(y, u(t))$ presents PDF, the equality $\int_a^\xi r(y, u(t)) dy = 1$ should hold for any $u(t)$ so that only n-1 weights are independent. So, (28) can be rewritten as

$$r(y, u(t)) = C(y)V(t) + e_0(y, u(t)) \tag{29}$$

where $C(y) = [B_1(y), B_2(y), \cdots, B_n(y)]$ and $V = [w_1, w_2, \cdots, w_n]^T$. To guarantee $\int_a^\xi r(y, u(t)) dy = 1$, the error $e_0(y, u(t))$ should be equal to zero.

According to (2), $w_{pi}(k+1)$ can be expressed by

$$w_{pi}(k+1) = w_{mi}(k+1) + w_{mi}(k) - w_i(k) = f^i(u(k)) + w_{mi}(k) - w_{oi}(k) \tag{30}$$

So, according to Eq.(3), the predictive PDF $r_p(y, u)$ can be rewritten as

$$r_p(k+1) = C(y)V_p(k+1) = \sum_{i=1}^n w_{pi}(k+1)B_i(y) = \sum_{i=1}^n [f^i(u(k)) + w_{mi}(k) - w_{oi}(k)]B_i(y) \tag{31}$$

As discussed above, it is obvious that $r_p(k+1)$ is only relative to reagent dosage $u(k)$ and random variable of bubble size y.

Corresponding to Eq.(29), a given desired PDF $r_g(y)$ can be expressed by

$$r_g(y) = \sum_{i=1}^n w_{gi}(u)B_i(y) = C(y)V_g \tag{32}$$

14

where V_g is the desired weight vector corresponding to the same basic function $B_i(y)$
($i = 1, 2, \cdots, n-1, n$).

The purpose of the controller design is that the reagent dosage $u(k)$ is regulated to make $r(y, u(k))$ follow $r_g(y)$. So the error between $r(y, u(k))$ and $r_g(y)$ can be formulated as

$$e_p(k+1) = r_g(y) - r_p(k+1) = \sum_{i=1}^{n} w_{gi} B_i(y) - \sum_{i=1}^{n} [f^i(u(k)) + w_{mi}(k) - w_{oi}(k)] B_i(y)$$

$$= \sum_{i=1}^{n} [w_{gi} - f^i(u(k)) - w_{mi}(k) + w_{oi}(k)] B_i(y) \tag{33}$$

Recently, the entropy concept has been widely used in stochastic systems (Wang, 2002; Guo and Wang, 2006). Since the entropy is the measure of randomness for a given random variable, entropy based controller can thus reduce the uncertainty of the closed-loop system. To minimize model uncertainties of the non-Gaussian stochastic systems, the performance function (Wang 2002) is selected as

$$\min J(u(k)) = \int_a^b e_p(k+1) \ln e_p(k+1) dy + \beta u(k)^2$$
$$= \int_a^b \{\sum_{i=1}^{n} [w_{gi} - f^i(u(k)) - w_{mi}(k) + w_{oi}(k)] B_i(y)\} \ln\{\sum_{i=1}^{n} [w_{gi} - f^i(u(k)) - w_{mi}(k) + w_{oi}(k)] B_i(y)\} dy + \beta u(k)^2$$

$$\tag{34}$$

It can be seen that the first term in (34) is the entropy at sample time k, while the second term is a natural quadratic constraint for the control input as reagent dosage. β is a prespecified number and $\beta > 0$. The following gradient descent based approach can also be used to calculate reagent dosage

$$u(k) = u(k-1) - \lambda \frac{\partial J}{\partial u}|_{u=u(k-1)} \tag{35}$$

where λ is a prespecified learning rate and $\lambda > 0$.

4 Experimental results and discussion

4.1 Hardware and network

A series of industrial experiments are carried out to implement tracking for the given PDF by the proposed method in a Chinese copper flotation plant. An image measurement device is mounted on the first cell of the roughing flotation to capture froth images. The measurement set-up is shown in Fig.5 (a). It consists of a RGB camera, a light source, a box hood, an optic fiber, an optical terminal, an image-transform card and an industry computer, etc. The RGB camera with 30mm lens and frame rate of 15 frames/s is installed 160cm above the surface of flotation froth layer.

It is noticed that the camera installation position is crucial to obtain high-quality images. The flotation machine with volume of 130 m³ and with highness of 8500ml in the plant are used to simplify flotation circuits and to improve their control capability. The cell includes internal launder and external launder to improve discharge capacity. Some researchers chose a position near the cell lip for focusing on the measurement of velocity. In this paper, a position between the cell lip and the cell center, which is slightly nearer the cell lip, seems to be better choice for the following two reasons. First, the position is chosen far from the cell center which has a great influence on bubble size structure when the impeller agitates slurry. Second, bubble size structure was easily distorted when concentrate overflow enters into the concentrate launder near the cell

15

tip.

The purpose of the box hood made by aluminum alloy is to act as a supporting structure for the measurement set-up as well as a protective element against dust coming from the flotation slurry, water which is used to clear flotation cell, corrosion coming from chemical reagents and the ambient light coming from the flotation hall. This is important since some image analysis algorithms need the total reflectance point on top of each bubble as a basis for further calculation.

The installed camera inside the hood is vertical to foam surface so that image geometry is perpendicular. And the high frequency electrodeless fluorescent lamp with illumination intensity of 1500 lux, color temperature of 4500k and frequency of 2.65M Hz is as parallel and closely near the camera as possible. This guarantees that single bubbles have only one total reflectance point, which is a very useful property for segmentation algorithms since they can use this bright spot as a starting point for bubble segmentation.

(a)   (b)
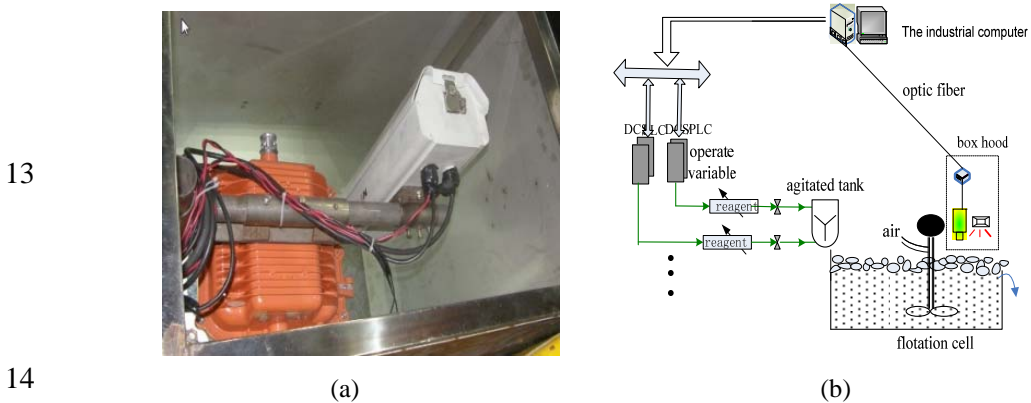
Fig.5 Measurement set-up and the industrial network diagram. (a) hardware configuration of image acquisition.(b) The industrial network diagram

The hard system network diagram is shown in Fig.5 (b).The camera is connected with the industrial computer through optic fiber. The industrial computer is connected with reagent system by OLE for process control (OPC). In the test runs, froth images are captured by the camera under the same condition in terms of resolution, angle, light condition, position, view scale, etc., and then transmitted to the industrial computer through optical fiber. Subsequently, the froth images are segmented into a large number of blobs namely blob set by the proposed watershed algorithm. The PDF of bubble size is then accurately depicted according to the blob set by entropy based B-spline technology. Finally, the industrial computer calculates the reagent dosage by the proposed method and then modifies chemical addition of reagent system by OPC.

In practice, the reagent is fed by electromagnetic valve of feeding bump in the reagent system. since the reagent flow rate and the dosing time are fixed, the chemical addition is capable to be altered only by altering dosing frequency. The reagent system calculates dosing frequency and then controls electromagnetic valve by PLC when the reagent dosage varies.

4.2 Flotation experiment

The ratio of reagents such as collector and frother has been determined by many practical flotation process experiments in the plant. The reagents are mixed to become a new reagent namely Z200 according to the ratio in reagent room. As mentioned above, the criterion of bubble size is closely related to the ore grade. So, in term of simplicity, it's necessary to remain less

1 fluctuation in ore property (i.e. $Grade_{ore} \in [0.95\% \ 1.01\%]$) during the experiment.

2 The parameters of the models including MLS-SVM model, reagent dosage optimization
3 model and B-spline model is determined before the proposed control method is applied to the
4 flotation experiment. Before the modeling phase of MLS-SVM, the systematic collection of
5 statistical data of copper flotation production was carried out. 500 groups of data were collected,
6 of which 420 groups were used to establish the MLS-SVM model, and the remaining 80 groups
7 for model validation. All these data were collected on ore grades of $[0.95\% \ 1\%]$ and normal

8 production conditions. The parameters of MLS-SVM model include the widths $\sigma^j(j=1,2,\cdots,n_y)$

9 of Gaussian kernel and the penalty coefficient $\gamma^j(j=0,1,2,\cdots,n_y)$, where $n_y = 9$. The selected

10 parameters are optimized by the PSO. For accelerating the search, we experimentally narrow the
11 boundaries of the parameters, where the penalty coefficients are initially set as an integer in [1,500]
12 due to the fact that integer is sensible enough to the predicted result. The widths of kernel are
13 initially set as a decimal ranged in [0.10–1.50]. Finally, the optimization value of the parameters is
14 obtained as follow: $\sigma = [1.08 \ 0.96 \ 0.83 \ 1.13 \ 1.01 \ 0.94 \ 0.89 \ 1.11 \ 0.79]$,
15 $\gamma = [201 \ 138 \ 148 \ 153 \ 259 \ 211 \ 197 \ 161 \ 98 \ 121]$.

16 In order to assess prediction performance, the root mean square error (RMSE)

17 $RMSE = \sqrt{\dfrac{1}{n}\sum\limits_{i=1}^{n}(\hat{y}_i - y_i)^2}$ and the correlation coefficient $R = \dfrac{\sum\limits_{i=1}^{n}(y_d - \bar{y})(\hat{y}_d - \bar{\hat{y}})}{\sqrt{\sum\limits_{i=1}^{n}(y_d - \bar{y})^2 \sum\limits_{i=1}^{n}(\hat{y}_d - \bar{\hat{y}})^2}}$ are adopted as the

18 evaluation indexes of accuracy of MLS-SVM, where y_i and $\hat{y}_i$ are actual and predicted

19 outputs, respectively, and $\bar{y}_i$ and $\bar{\hat{y}}_i$ are averages of actual and predicted outputs, respectively,

20 n is the amount of predicted points. In the experiments, the RMSE and the correlation coefficient
21 of weights are respectively calculated as RMSE=[0.0605 0.0550 0.0416 0.0734 0.0361 0.0945
22 0.0378 0.0643 0.0888] and R=[0.9557 0.9458 0.9470 0.9610 0.9582 0.9816 0.9883 0.9407
23 0.9810]. It is obvious that they are capable to meet predictive requires of MLS-SVM.
24 As discussed in section 3.2, the number of base function determined by minimizing entropy
25 is nine in B-spline model unit. In reagent dosage optimization unit, the coefficient λ of the
26 gradient descent is obtained as $\lambda = 0.7$.
27 Through analysis for a large amounts of process data and expert knowledge, the given weight
28 vector, which is likely optimal PDF of industry flotation foam in the same condition as ore
29 property, is set to be: $V_g = [2.2287 \ 2.8708 \ 2.4107 \ 1.3445 \ 0.3397 \ 0.1240 \ 0.1338 \ 0.039 \ 0]$.
30 Suppose that the initial weight vector values of flotation bubble PDF is
31 $V_0 = [2.1912 \ 2.5821 \ 1.5448 \ 0.7055 \ 0.4878 \ 0.4643 \ 0.4562 \ 0.5362 \ 0.4740]$
32 Suppose that the weight vector of the PDF of bubble size of is V_0 when some disturbance
33 occurs in roughing flotation at 9:00 on September 20. At the same time the reagent flow rate is
34 180ml/min and the pulp level is -200mm. In order to implement tracking for V_g, the PDF of the
35 output bubble size need to be measured and the reagent dosage is then calculated by the proposed
36 method every 5 minutes. The output of the reagent dosage predictive control model is shown in

Fig.6. In Fig.6 (a)-(i), the blue lines represents weight value of the PDF of the output bubble size and the red lines represents the predictive weight value of MLS-SVM at time k. The black lines represents the given weight value. In Fig.6 (j), the blue line represents the predictive value of the reagent dosage optimization model and the red line represents the corresponding value of pulp level at time k. It is concluded in Fig.6 that the proposed method is capable to implement tracking for the targeted PDF.

(a)

(b)

(c)

(d)

(e)

(f)

(g)　　　　　　　　　　　　　　　(h)

2

3　　　　　　　　　　(i)　　　　　　　　　　　　　　　(j)
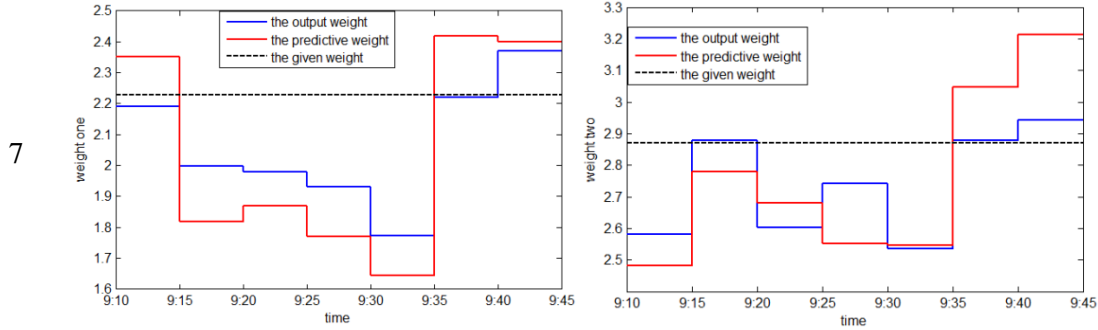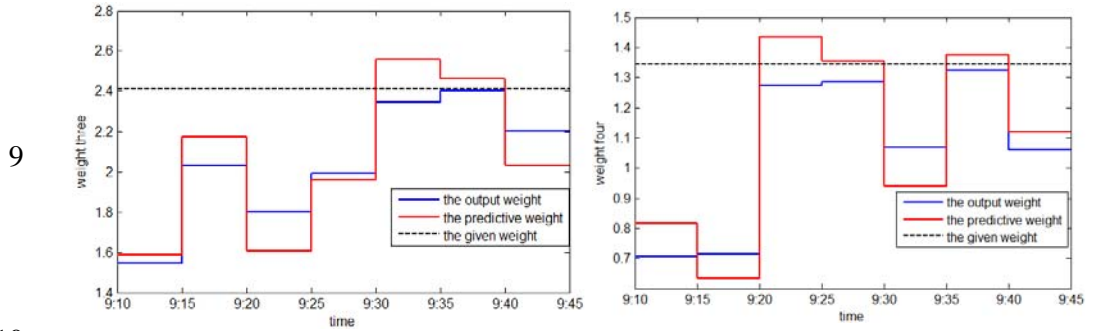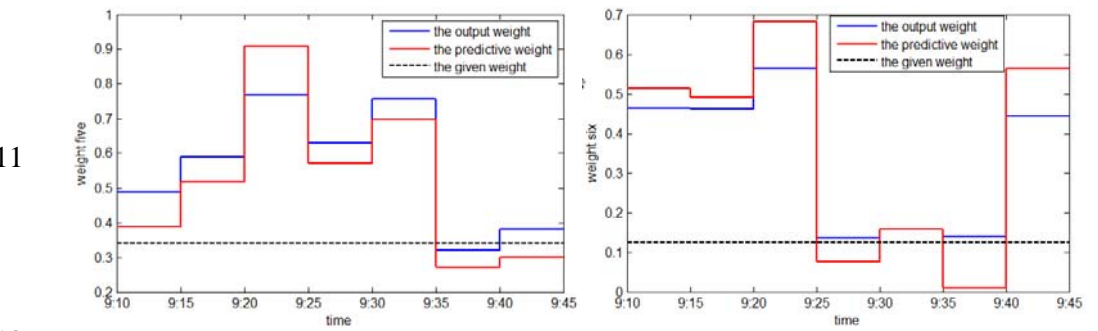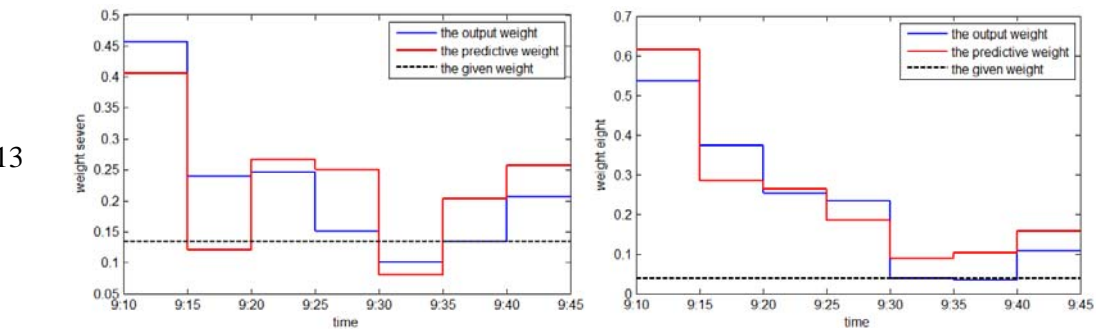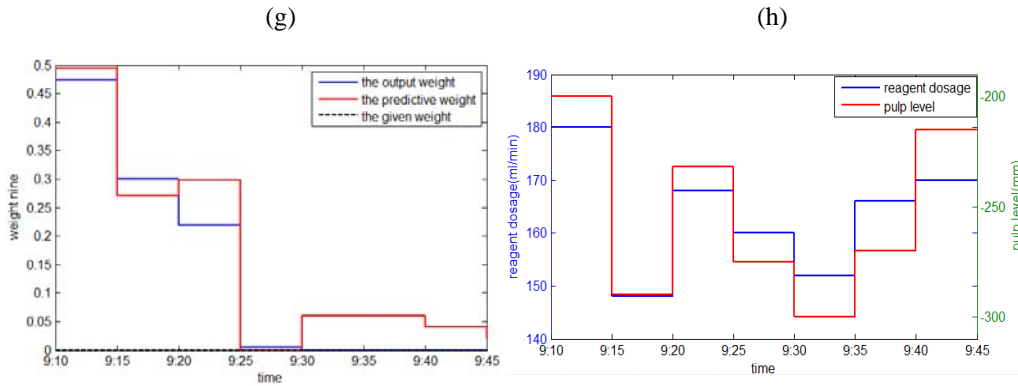
4　　　　　　　Fig.6 Weighs tracking and predictive reagent dosage

5　　　At the same time, the evolution of the froth images in the first cell of roughing flotation is

6　shown in Fig. 7. Fig. 7 (a) and (b) represents the 2-D and 3-D plot of weights tracking evolution,

7　respectively.

8

9　　　　　　　　　(a)　　　　　　　　　　　　　　　(b)
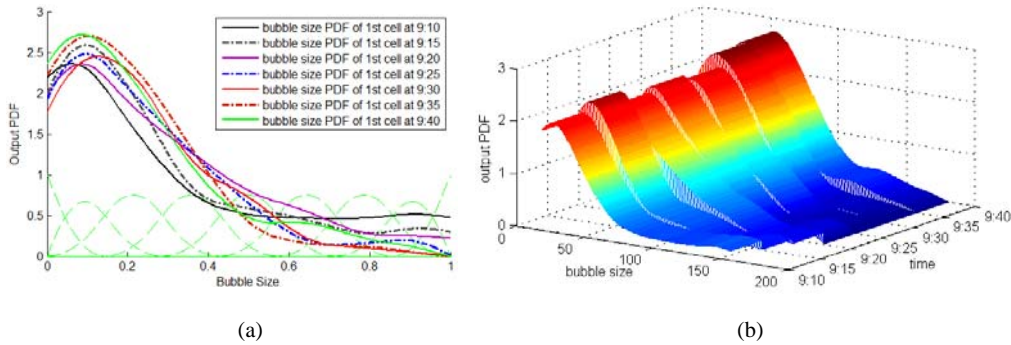
10　Fig.7. weights tracking evolution from the initial PDF to the given PDF after reagent dosage is altered. (a) the

11　　　　2-D plot of weights tracking evolution (b) the 3-D mesh plot of weights tracking evolution

12　4.3 Results discussion

13　　　In the flotation plant, the operators are most concerned about the production indices since the

14　indices are closely related to employee performance evaluation. To evaluate the effectiveness of

15　the proposed method, it is suggested that the production indices produced by the proposed method

16　compare with those produced by the workers. Moreover, the reagent dosage expended by the

17　proposed method is also compared with those expended by the workers. At present, three shifts 18 including morning shift (0:00~8:00), afternoon shift (8:00~16:00) and night shift (16:00~24:00) 19 are scheduled in the plant. Generally, the process experiment using the proposed method is

20　arranged during afternoon shift, the flotation productions using manual mode are arranged during

21　the other shifts. During afternoon shift, the reagent dosage is regulated according to the PDF of the

22　output bubble size. If the adjusted reagent increment (or decrement) is larger than 20ml/min, the

23　control system sounds an alarm and inform the workers that the pulp level of flotation machine 24 may need to be regulated. The workers then observe the froth image and regulate the pulp level by 25 the monitoring system. During morning and night shift, the workers inspect(巡视) flotation

26　process every one hour. When the workers observe the froth and consider that the bubble size does 27　　not meet his criteria for good bubble size, they will regulate the reagent dosage and the pulp level

1   by reagent control panel. It is noticing that the workers need repeatedly regulate the reagent

2   dosage and the pulp level by observing the bubble size until the output bubble size meet their 3

criteria. Generally, the flotation parameters don't change from one shift to the next shift. So, the 4

reagent dosage and the pulp level will be regulated from afternoon shift to night shift only when 5

the workers inspect flotation process and find flotation abnormalities. The reagent dosage is 6

regulated according to the changing bubble size every several minutes from morning shift to 7

afternoon shift.

8   As discussed in the paper, the feed grade and the other feed parameters (such as the

9   feed flow rate, the solid constant, the pH and the mineral size distribution) are considered as a 10

prerequisite and disturbance variables for flotation, respectively. The operation parameters such as 11

the reagent dosage and the pulp level are regulated variables for flotation. The feed flow rate, the 12

pH, the pulp level and the reagent dosage are capable to be obtained by OPC all the time. The 13

grade (such as feed grade, concentrate grade and tailing grade), the solid percent and the particle 14

size of solid need to be obtained by assay. However, the workers do not assay the parameters other 15

than the grade since the flotation state is determined by observation of bubble size during the 16

experiment. So, it is shown in Fig. (8) that the obtained experimental data of every shift include 17

the feed grade, the handling capacity, concentrate grade, recovery and reagent dosage. It is seen in 18

Fig. 8 (a) that the feed grade varied from 0.95% to 1.01%. It is seen in Fig. 8 (b) that the handling 19

capacity is fluctuated from 4065 ton to 4396 ton. It is seen in Fig. 8 (c) that the fluctuation of 20

grade of afternoon shift is less than that of the other shifts, and the grade of afternoon shift is

21   relatively higher than that of the other shifts. It is seen in Fig. 8 (d) that the fluctuation of recovery

22   of afternoon shift is less than that of the other shifts, and recovery of afternoon shift is relatively

23   higher than that of the other shifts. However, it is shown in Fig. 8 (e) that the consumption and 24

fluctuation of reagent dosage of afternoon shift are less than those of the other shifts. It is

25   indicated in Fig. 8 that using the proposed method is capable to make flotation running more
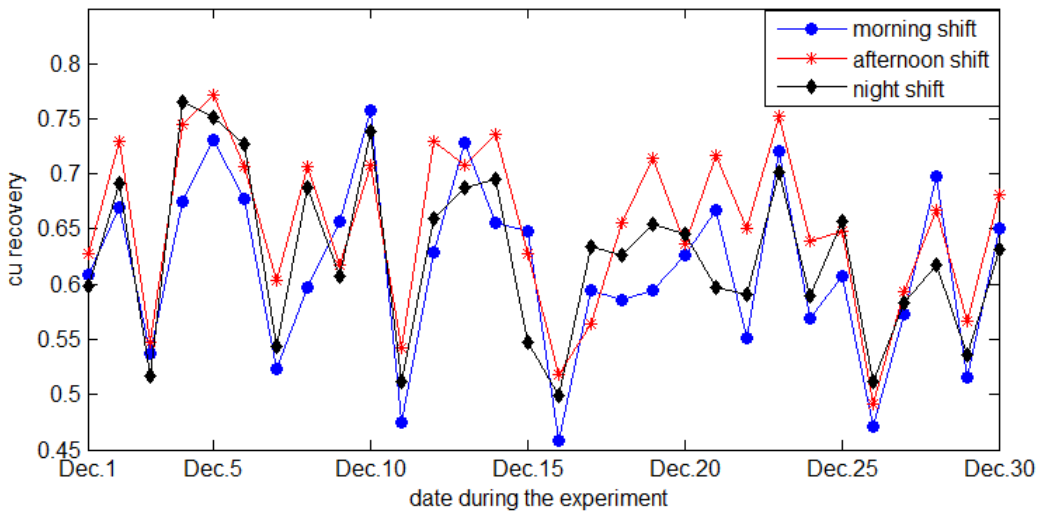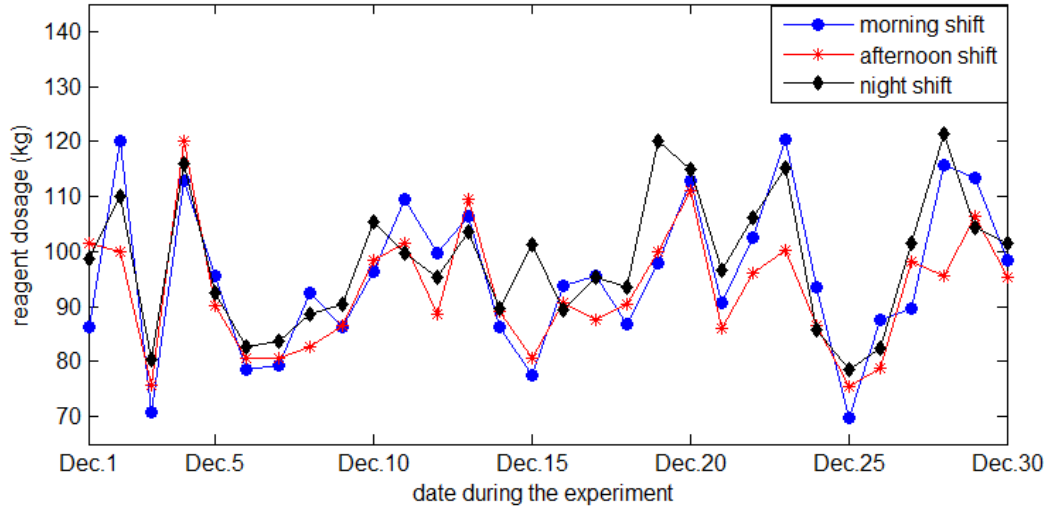
26   stable than using manual operation.

27

1

2

3
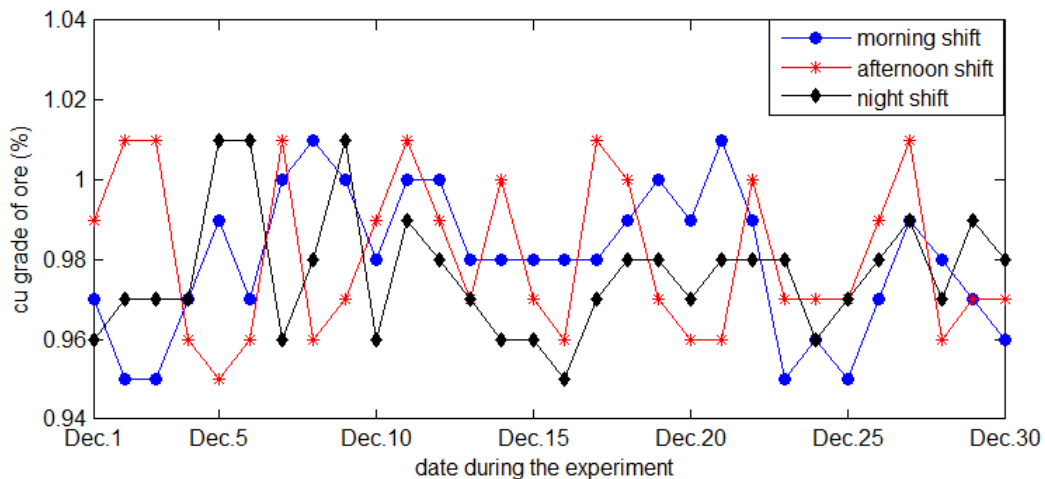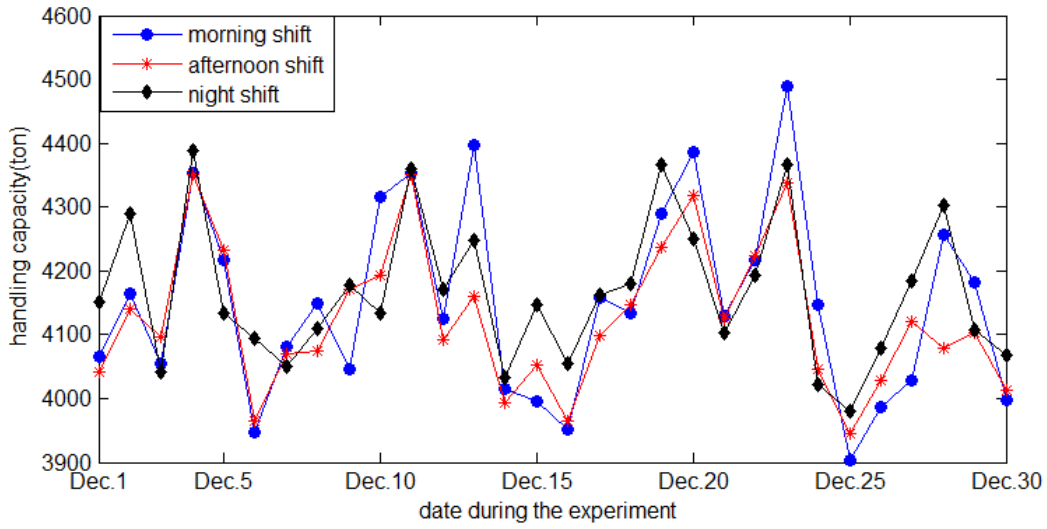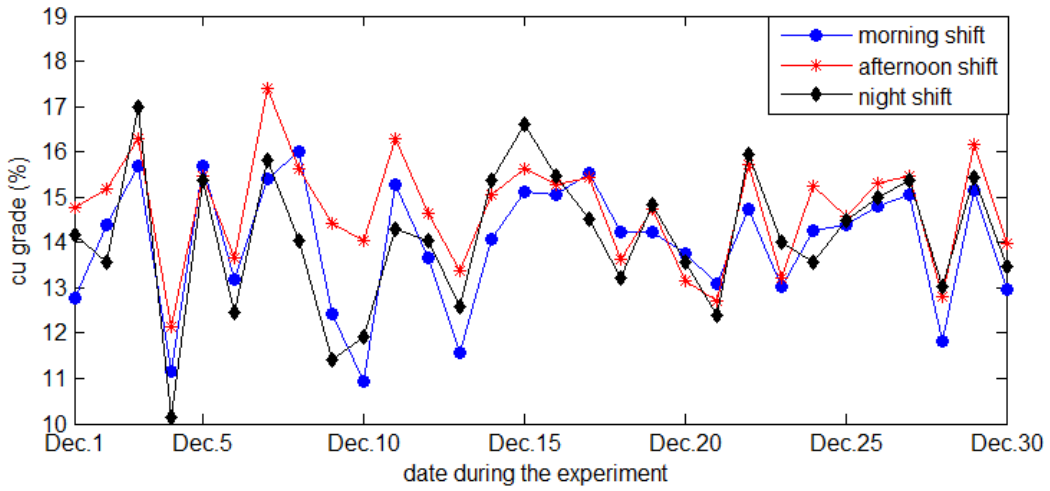
Fig. 8 Feed grade, Handling capacity, Grade, recovery and reagent dosage of every shift during the experiment. (a) cu grade of ore. (b) handling capacity. (c) cu grade.(d) cu recovery. (e) reagent dosage

The eligible grade and recovery need to be larger than 14% and 0.55 for the copper rougher, respectively. Table 1 shows the amount of the eligible indices during the experiment and the consumption of the Z200. The amount of the eligible recovery of afternoon shift, morning shift and night shift is respectively 26, 24 and 23 during the experiment. The amount of the eligible grade of afternoon shift, morning shift and night shift is respectively 21, 18 and 18 during a month. The reagent consumption of afternoon shift, morning shift and night shift has respectively 2758.18 kg, 2874.28 kg and 2943.97 kg during a month. It is obvious that the eligible indices amounts of afternoon shift are more than those of morning shift and night shift. However, the reagent consumption of afternoon shift decrease 116.1kg and 185.79 kg than that of morning shift and night shift, respectively. Expect for more qualified recoveries and grades, more economy benefit is also produced by the proposed method.

Table 1 evaluation indices of every shift during a month

	Amount(percept) of recovery larger than 0.55	Amount(percept) of grade larger than 14%	Reagent(Z200) dosage in a month(kg)
afternoon shift (the proposed method)	87%	70%	2758.18
morning shift (manual mode)	80%	60%	2874.28
night shift (manual mode)	77%	60%	2943.97

5 Conclusion and future work

First of all, process description of copper flotation is presented and modeling analysis of reagent dosage control is discussed in this paper. A PDF based reagent dosage predictive control structure is then proposed. The structure consists of a measurement unit, a MLS-SVM unit, a feedback correction unit and a reagent dosage optimization unit. The captured froth images is segmented by the two-pass watershed algorithm and the PDF of bubble size is depicted by entropy

based B-spline technology in the measurement unit. Since the PDF is characterized by weights of B-spline, controlling for BSD is transformed into controlling for discrete weights. The dynamic relationship between the reagent dosage and the PDF of bubble size is built by MLS-SVM. The reagent dosage is optimally calculated by entropy based optimization algorithm. Finally, the hardware, the camera installation position and the system network is discussed and then the flotation experiment is presented to implement tracking control for the output PDF of bubble size using the proposed algorithm. Experimental results are presented to show the effectiveness of the proposed method. Note that the unexpected emergency of the flotation sometime need manual intervention mode to guarantee the safety of production during the experiment period.

As a future work, a similar multi-camera system should be installed into other circuit of the copper flotation, including the last cell of the cleaning and the scavenging. Data collection and analysis campaign will be launched. Based on subsequent data analysis of all circuits, appropriate updates will be done to reagent dosage controller in the copper flotation, and performance of the updated controller will be analyzed. Another a important area for future work is the accurate measurement of froth texture. Data analysis done so far has shown that texture and bubble size can be strongly correlated with the grade. Based on two dimension relation with bubble texture and size using the joint probability density distribution, How reagent addition control is well accomplished? In addition, abnormal flotation states such as froth outflow, pulp upturn and low pulp level, etc. sometimes occur for some reasons during flotation running. Data-driven based fault detection and isolation (FDI) and fault-tolerant control (Yin, Luo, Ding, 2013) for flotation will be good and interesting topics since control and FDI in the identical framework will further the system integration of control and FDI for mineral flotation, which is beneficial for better flotation running. As such, this will be one of our future topics.

Acknowledgements

References

Bartolacci G, Serranti S, Volpe F, Zuco R (2001). Characterization of flotation froth structure and color by machine vision [J]. Computers and Geosciences, 27(9): 1111-1117.

C. Aldrich and D. Feng (2000). The effect of frothers on bubble size distribution in flotation pulp phases and surface froths. Minerals Engineering, Vol. 13, No. 10-1, 1049-1057.

Canhui Xu, Weihua Gui, etc (2012). Flotation process fault detection using output PDF of bubble size distribution[J]. Minerals Engineering Volume 26, January, Pages 5-12.

C. P. Botha (1999). An on-line machine vision flotation froth analysis platform. Master's thesis, University of Stellenbosch.

E. H. Girgin, S. Do, C.O. Gomez, J.A. Finch (2006). Bubble size as a function of impeller

speed in a self-aeration laboratory flotation cell. Minerals Engineering, 19 201-203.

Gordon Forbes (2007).Texture and Bubble Size Measurements for Modelling Concentrate Grade in Flotation Froth Systems[D] . university of cape town. 106~119.

Hodouin, D. Flament etc. (2000) Feedforward-feeedback predictive control of a simulated flotation bank. Power technology, 108 173-179.

Hodouin, S. L. Jamsa-Jounela, M. T. Carvalho, L. G. Bergh (2001). State of the art and challenges in mineral processing control, Control Engineering Practice 9 995-1005.

Hong Wang (2002). Minimum Entropy Control of Non-Gaussian Dynamic Stochastic Systems. IEEE Transaction on automatic control, vol. 47, no.2, February.

Hong Wang (2000). Bounded Dynamic Stochastic Distributions Modelling and Control, Springer-Verlag, London.

J. Kaartinen, J. Miettunen, etc. (2006). Machine-vision-based control of zinc flotation-a case study, Control Engineering Practice, 14 1455–1466.

K. Runge, J. McMaster, M. Wortley, D. L. Rosa, and O. Guyot (2007). A correlation between visiofroth measurements and the performance of a flotation cell. In Ninth Mill Operators' Conference, pages 19–21, Fremantle, Western Australia.

L.G. Bergh, J.B. Yianatos (2011). The long way toward multivariate predictive control of flotation processes. Journal of Process Control, 21 226–234.

Lei Guo, Hong Wang (2010). Stochastic distribution control system design. Springer-Verlag, London.

Lei Guo and Hong Wang (2006). Minimum entropy filtering for multivariate stochastic systems with non-Gaussian noises. IEEE Transaction on automatic control, vol.51, no.4, April.

Liu J, Gui W, Tang Z, et al. (2013). Recognition of the operational statuses of reagent addition using dynamic bubble size distribution in copper flotation process[J]. Minerals Engineering, 45: 128-141.

Liu J. J., Macgregor J F, Duchesene C, Bartolacci G (2005). Flotation froth monitoring using multiresolutional multivariate image analysis [J]. Minerals Engineering, 18(1): 65-76.

M.G. Forbes, M. Guay, J.F. Forbes (2004). Control design for first-order processes: shaping the probability density of the process state[J]. Journal of Process Control, 14 399-410.

M. Suichies, D. Leroux, C. Dechert, A. Trusiak (2000). An implementation of generalized predictive control in a flotation plant. Control Engineering Practice, 8 319-325.

Neethling, S.J. Lee, H.T. Cilliers, J.J. (2003). Simple relationships for predicting the recovery of liquid from flowing foams and froths. Minerals Engineering 16 (11), 1123-1130.

P. K. Naik, P. Sita Rama Reddy, Vibhuti N, Misra (2005). Interpretation of interaction effects and optimization of reagent dosage for fine coal flotation. Int. J. Miner. Process, 75 83-90.

R. A. Grau, K. Heiskanen (2005). Bubble size distribution in laboratory scale flotation cells. Minerals Engineering, 18 1164-1172.

S. Xu, X. An, etc. (2013). Multi-output least-squares support vector regression machines. Pattern Recognition Letters, 34 1078-1084.

S. Yin, S. X. Ding, A. Haghani, et al. (2012). A comparison study of basic data-driven fault diagnosis and process monitoring methods on the benchmark Tennessee Eastman process[J].

Journal of Process Control. 22(9), 1567-1581.

S. Yin, H. Luo, S. Ding (2013). Real-time implementation of fault-tolerant control systems with performance optimization[J]. IEEE Transactions on Industrial Electronics, doi: 10.1109/TIE.2013.2273477.

W. Wang, F. Bergholm, and B. Yang (2003). Froth delineation based on image classification. Minerals Engineering, 16:1183–1192.

Wang Wei-xing, Li Lei (2005). Image analysis and computer vision for mineral froth Proceedings of IEEE International Conference on Mechatronics and Automation. Niagara Falls, Canada: 1790-1795.

Wang, Y., & Neethling, S. J. (2009). The relationship between the surface and internal structure of dry foam. Colloids and Surfaces A: Physicochemical and Engineering Aspects, 339 (1), 73-81.

X.C. Guo, J. H. Yang, etc. (2008). A novel LS-SVMs hyper-parameter selection based on particle swarm optimization. Neurocomputing, 71 3211-3215.

Y.S. Cho, J.S. Laskowski (2002). Effect of flotation frothers on bubble size and foam stability. Int. J. Miner. Process, 64 69-80.

Yang, C., Xu, C., Gui, W., Du, J. (2009). Nonparametric density estimation of bubble size distribution for monitoring mineral flotation process. In: 48th IEEE Conference on Decision and Control, Shanghai, pp. 2941-2945.

Yang, Y., Guo, L., & Wang, H. (2009). Constrained PI tracking control for output probability distributions based on two-step neural networks. IEEE Transactions on Circuits Systems Part I, 56(7), 1416-1426.

Z. Zong, K.Y. Lam (1998). Estimation of complicated distributions using B-spline functions. Structural Safety, 20 341-355.

Z. Y. Han, Y. Liu, etc. (2012). Real time prediction for converter gas tank levels based on multi-output least square support vector regressor. Control Engineering Practice, 20 1400-1409.